

Audio-Visual Camera Pose Estimation with Passive Scene Sounds and In-the-Wild Video

Daniel Adebi Sagnik Majumder Kristen Grauman
University of Texas at Austin

{ikadebi, sagnik, grauman}@cs.utexas.edu

Abstract

Understanding camera motion is a fundamental problem in embodied perception and 3D scene understanding. While visual methods have advanced rapidly, they often struggle under visually degraded conditions such as motion blur or occlusions. In this work, we show that passive scene sounds provide complementary cues for relative camera pose estimation for in-the-wild videos. We introduce a simple but effective audio-visual framework that integrates direction-of-arrival (DOA) spectra and binauralized embeddings into a state-of-the-art vision-only pose estimation model. Our results on two large datasets show consistent gains over strong visual baselines, plus robustness when the visual information is corrupted. To our knowledge, this represents the first work to successfully leverage audio for relative camera pose estimation in real-world videos, and it establishes incidental, everyday audio as an unexpected but promising signal for a classic spatial challenge. Project: http://vision.cs.utexas.edu/projects/av_camera_pose.

1. Introduction

Consider a video captured at a dark, crowded concert where someone wearing a camera moves through the venue searching for friends near the stage. The visual feed is severely degraded by dim lighting, motion blur, and constantly shifting crowds, making it difficult to track camera movement through vision alone. Yet the surrounding audio tells a clear spatial story: music grows louder as the person approaches the stage and the music shifts as they turn their head; conversations fade in and out with proximity; and ambient crowd noise provides persistent directional cues.

Could a *camera pose estimation model* use such incidental sounds in real-world video to refine its spatial story too? This goal is appealing for multiple reasons. First, incidental *passive* scene sounds are compelling because—unlike actively emitted chirps for echolocation [10, 17, 65]—they are non-intrusive, varied, and freely available with video.

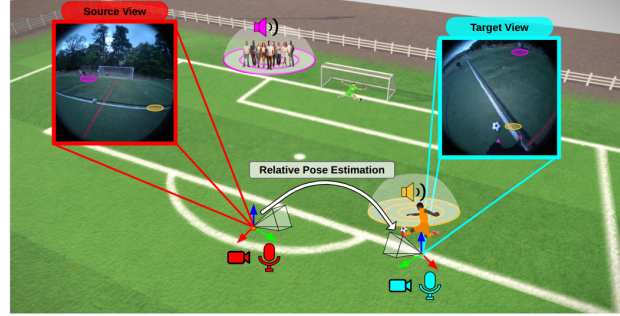


Figure 1. **Main idea:** we propose to estimate relative camera pose from in-the-wild videos using both vision and multichannel audio. Unlike traditional active echolocation sensing, our model relies only on passive scene audio—gaining spatial cues opportunistically from naturally occurring ambient and foreground sound sources.

Second, everyday sounds are invariant to some of the key obstacles for traditional vision-only camera pose estimation, like poor lighting, motion blur, textureless regions, and occlusions. Audio’s geometric cues remain reliable even when vision fails.

Motivated by these observations, we introduce an audio-visual camera pose estimation model. Given two video frames and their respective multi-channel audio excerpts, the objective is to predict the relative camera pose separating the two frames. See Figure 1. Building on a state-of-the-art vision-only model [14], we introduce a joint audio representation comprised of explicit direction-of-arrival audio cues and a mono-to-binaural “lifted” embedding. Importantly, we train entirely with real-world video from a variety of scenarios and activities—a significant departure from the status quo, where methods exploring spatial audio rely on static (usually 3D-scanned [46, 53]) environments and simulated audio [7, 9, 15, 17, 45, 65].

We validate our approach on two datasets. Our model achieves significant improvements, outperforming the state-of-the-art [9] and establishing (to our knowledge) the first-ever results for audio-visual camera pose estimation on challenging real-world videos. Our key contributions are:

- We introduce a spatial audio encoder that learns spatial embeddings from two complementary cues: direction-of-arrival spectra and cross-view audio binauralization features.
- We validate our approach on the large-scale Ego-Exo4D dataset [20] containing hundreds of subjects and environments and the HM3D-SS [7, 46] dataset, achieving state-of-the-art performance among audio-visual baselines for relative camera pose estimation.
- We provide a comprehensive analysis of how different audio characteristics affect multimodal camera pose estimation.

Overall, our work establishes incidental, passive audio as a promising signal for camera pose.

2. Related Work

We review related work on audio-visual learning.

2.1. Vision-based camera pose estimation

Accurate relative camera pose estimation is fundamental to a wide range of applications in 3D vision, augmented reality, and robotics. Most camera pose estimation methods rely solely on visual information [5, 13, 14, 30, 47, 49, 58–61, 68, 69]. Earlier methods such as SuperGlue [49] and LoFTR [54] rely on correspondence through keypoint matching, which makes them well suited to scenarios with high degrees of visual overlap between images. More recent approaches like DUSt3R [59] and Reloc3r [14] leverage end-to-end transformer architectures, allowing direct correspondence estimation without relying on explicit keypoint detection and matching. FAR [47] integrates feature matching with learning-based approaches to improve performance under low visual overlap scenarios. Other methods incorporate depth [13, 69] and optical flow [61] to further improve the performance.

All these methods rely solely on visual input for camera pose prediction, leveraging training data that spans simulated environments [24, 44, 50, 53, 56], reconstructed 3D scans of real scenes [4, 6, 11, 66, 67], photographs of static real-world environments [3, 25, 29, 35, 52, 57], and real-world videos [12, 27, 55, 63, 70]. In our work, we incorporate audio as an additional modality to support pose estimation.

2.2. Echolocation for camera poses

To our knowledge, the only prior work to leverage audio for camera pose estimation does so in a very different setting—by actively emitting sounds into the environment in order to collect echoes [65]—and is limited to training and testing in simulation. Furthermore, no prior work uses passive scene audio for relative camera pose estimation. Our method relies solely on naturally occurring sounds already present in the scene, without emitting signals, generating new sounds in a simulated scene, or requiring controlled acoustic conditions,

making it passive, unobtrusive, and compatible with real-world videos.

2.3. Localizing sound sources

Leveraging both sound and vision to localize sound sources has emerged as a powerful strategy [9, 26, 33, 62]. Recent work shows how camera motion can reinforce estimates of sound source locations [9, 33]. Results are done in simulation [9] or using real-world video egomotion to supervise binaural sound localization [33]. In related spatial problems, audio-visual models can learn floorplan maps [45] and 3D scene structure [10] by associating sounding objects with likely rooms and/or listening for echolocation responses. Other work trains navigation policies to move to a sounding object in an unmapped environment [7, 15]. Unlike any of the above, our aim is to compute accurate 6 DoF relative camera poses, not sound source locations or environment maps.

2.4. Audio-visual self-supervised pretraining

Extensive prior work investigates how vision and audio interact to learn self-supervised representations, using the two modalities to create pretext tasks and improve training [1, 2, 23, 36, 38–41]. These studies build tasks around synthesis [40, 41], cross-modal alignment [1, 2, 17, 23, 39], and masked auto-encoding approaches [18, 19, 22], typically targeting semantic downstream problems such as audio-visual event classification and retrieval. Different from these objectives, our approach incorporates spatial audio-based representations into camera pose estimation.

3. Task motivation and definition

The spatial sound perceived in a 3D scene is shaped by the relative location and orientation of the microphones used in capturing the sound, relative to the sound source(s), as well as the scene’s geometry and materials. Consequently, any translation and/or rotation of the microphones results in changes in the sound’s spatial attributes, which reveal the nature and extent of microphone motion. Based on this knowledge, we hypothesize that leveraging spatial audio in addition to vision for relative camera pose prediction in in-the-wild videos—where the audio is captured using multiple microphones that move rigidly with the camera—can improve the pose prediction quality over using vision alone. We anticipate audio to be particularly valuable when vision alone is unreliable due to factors like occlusion, bad lighting, or camera failure, which are common in real-world video.

To validate our hypothesis, we propose a novel audio-visual in-the-wild relative camera pose estimation task. In this task, we consider a video clip $V = (I, A)$, where I and A denote the visual and multi-channel audio streams, respectively. The visual stream I consists of N RGB image

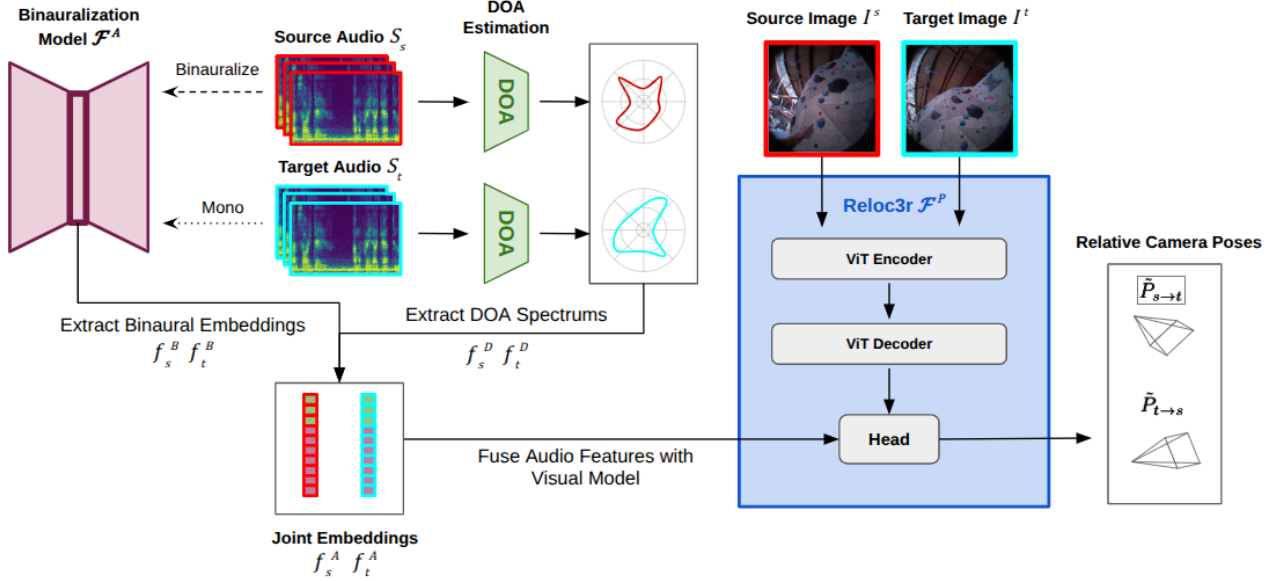


Figure 2. We extend the Reloc3r [14] architecture by incorporating both analytical and learned audio embeddings extracted using our Spatial Audio Encoder (SAE). Given a pair of source and target frames, coupled with their corresponding synchronized audio clips, our modified Reloc3r network predicts relative camera poses for the input image pair, in both directions (from source to target, and from target to source). The SAE produces a combination of analytical and learned spatial audio embeddings that are subsequently integrated with Reloc3r’s visual features via late fusion, enabling the network to leverage complementary audio-visual cues for performing high-quality pose prediction. This design allows joint learning of translation and rotation and additionally provides robustness to situations with varying degrees of visual corruption, as we show in results.

frames, such that $I = \{I_1, \dots, I_N\}$. The audio stream A is time-synchronous with I and consists of N audio segments, such that $A = \{A_1, \dots, A_N\}$. Each audio segment A_j has C audio channels, such that $A_j = \{A_j^1, \dots, A_j^C\}$, and is extracted by sampling a fixed-length time window (1000ms) centered at frame I_j , making A_j temporally aligned with V_j .

We make no assumptions about the audio other than it being captured from two (or more) microphones co-located with the camera.¹ In particular, we are interested in leveraging *passive* sounds—whatever are the incidental sounds in the scene from various sources, foreground or background—as opposed to *active* sounds emitted into the environment to perform sensing, i.e., for echolocation. The advantage of passive sounds is that they are non-intrusive and “free”, and available even on previously recorded video over which our models have no control.

Given a pair of source and target RGB frames (I_s, I_t) and their corresponding multi-channel audio segments (A_s, A_t), the goal in this task is to learn a model \mathcal{F} , such that $\mathcal{F}(I_s, A_s, I_t, A_t) = \tilde{P}_{s \rightarrow t}$, where $\tilde{P}_{s \rightarrow t}$ is an estimate of the 6-DoF relative camera pose $P_{s \rightarrow t}$ between I_s and I_t . The matrix $P \in \mathbb{R}^{3 \times 4}$ represents the rotation and translation

¹We use the terms spatial audio and multi-channel audio interchangeably, to refer to audio captured from two or more microphones.

of the pose change. By augmenting the vision with audio, we aim for more accurate camera pose estimates, particularly when the visual stream is noisy and unreliable. Next, we describe our method in detail.

4. Approach

Our method is composed of two modules: **1**) a spatial audio encoder \mathcal{F}^A , and **2**) an audio-visual relative camera pose predictor \mathcal{F}^P . See Fig. 2. While the audio encoder \mathcal{F}^A is responsible for extracting rich spatial cues from the multi-channel audio inputs by using both analytical and learned representations, the pose predictor \mathcal{F}^P combines these spatial audio cues with visual cues using a SOTA camera pose prediction backbone [14] to estimate the relative camera pose. Next, we describe the design of these modules and their training.

4.1. Spatial audio encoder

Given any multi-channel audio segment A_j (cf. Sec. 3), our spatial audio encoder \mathcal{F}^A first computes a short-time Fourier transform (STFT) and represents the audio as a spectrogram S_j . S_j is a matrix, such that $S_j \in \mathbb{R}^{C \times F \times W}$, where F and W are the number of frequency bins and time windows, respectively, and C is the number of audio channels (e.g.,

$C = 2$ for binaural audio). We compute two representations from the spectrogram: the direction-of-arrival (DoA) and a learned spatial audio embedding. For the former, we use an analytical direction-of-arrival (DoA) estimator [48] to compute $f_j^D = \mathcal{F}^D(S_j)$, such that $f_j^D \in \mathbb{R}^{360}$. This DoA spectrum explicitly captures the distribution of sound energy around the microphone location, revealing the direction(s) of major sound sources in the environment with respect to the camera. For the latter, we compute a binaural audio embedding $f_j^B = \mathcal{F}^B(S_j)$ using a learned extractor (defined below) to provide an implicit but strong representation of the audio’s spatial characteristics.

Finally, the encoder fuses f_j^D and f_j^B into a spatial audio embedding f_j^A . The joint embeddings for the audio from both the source and target poses are passed to the camera pose predictor \mathcal{F}^P for further processing. Whereas the DoA feature f_j^D signals the direction of major sound sources in the surroundings, the binaural audio features capture the full fabric of all overlapping sounds and their spatial layout. The synergy of these two complementary features, enabled by their fusion, is essential for high-quality pose prediction, as we show in results. Next, we elaborate on the design of these encoders and our feature fusion strategy.

Direction-of-arrival spectrum. For our direction-of-arrival (DoA) feature, we use the MUSIC [51] algorithm with frequency normalization [48], henceforth referred to as MUSIC++. This method has been shown to produce reliable DoA estimates in the presence of multiple sound sources. Given a multi-channel audio-spectrogram S_j , MUSIC++ analytically computes a one-dimensional DoA feature f_j^D , such that $f_j^D \in [0, 1]^{360}$ and each entry measures the average audio intensity across the corresponding 1° -wide sector in the azimuth circle. In essence, f_j^D captures the angular variation in the audio intensity relative to the direction in which the microphones are facing. Notably, this DoA distribution will shift predictably as a function of the camera’s motion—and vice versa—provided there are not sudden changes in the scene sounds between the time frame I_s and I_t are captured (1 sec. in our experiments).

Learned binaural audio features. Inspired by prior work for self-supervised audio(-visual) learning [8, 9, 16, 17, 32, 37, 42, 64], we train an embedding to lift monaural to binaural sound in the target viewpoint. Specifically, we train \mathcal{F}^B by attempting to solve a novel viewpoint² (view) acoustic synthesis (NVAS) task, where given a pair of views—one source and one target, the goal is to learn a model that can take the binaural audio for the source view and the monaural audio for the target view, as inputs and generate the binaural audio for the target view. By training the NVAS model on a large and challenging dataset [20] comprising a large variety of dynamic 3D scenes with multiple overlapping sound

sources at diverse locations and ambient noise, and arbitrary viewpoint changes, \mathcal{F}^B learns to encode rich spatial audio features.

To instantiate the NVAS task, we convert each multi-channel audio spectrogram S_j into its binaural counterpart S_j^B using the SOFA [43] toolbox. Specifically, SOFA first computes the spectrogram’s monaural variant S_j^M by averaging across all C channels and then convolves S_j^M with a head-related transfer function (HRTF) to obtain the binaural spectrogram S_j^B . We use the monaural spectrogram S_j^M produced by SOFA during its first stage, as the monaural audio input for the NVAS model. Once the NVAS model is trained, we encode any multi-channel spectrogram S_j by first converting it into a binaural spectrogram S_j^B as discussed above and then feeding S_j^B into the binaural encoder \mathcal{F}^B to obtain its one-dimensional binaural feature f_j^B .

Spatial audio feature fusion. To leverage the complementary benefits offered by these two features, we fuse f_j^D and f_j^B into a single spatial audio feature f_j^A through concatenation, such that $f_j^A = [f_j^D || f_j^B]$. Our fusion strategy, coupled with the use of non-linearities in the subsequent model layers (see Sec. 4.2), allows for full feature mixing, making the fused features highly expressive and conducive to high-quality camera pose estimation.

4.2. Audio-visual relative camera pose predictor

For predicting the relative camera pose estimate \tilde{P} , we adapt a state-of-the-art vision-only relative camera pose predictor, Reloc3r [14], such that it can take both visual and spatial audio inputs. Given a pair of RGB images (I_s, I_t) , the original Reloc3r model processes them using a pair of visual branches with the exact same architecture and shared weights, in order to predict their relative camera poses in both directions, $\tilde{P}_{s \rightarrow t}$ and $\tilde{P}_{t \rightarrow s}$. Towards that goal, it feeds each image to just one branch, which extracts visual features from the image using an encoder-decoder pair. Additionally, it uses cross-attention between the decoders of the two branches to establish fine-grained spatial correspondences between the corresponding visual features. It then uses a stack of linear layers as its camera pose prediction head, which leverages the aforementioned correspondences and estimates the camera pose of each input image relative to the other.

To adapt Reloc3r for audio-visual inputs, we feed an audio-visual feature f^{AV} to the camera pose estimation head of each branch, where f^{AV} is produced by concatenating the head’s original input feature f^V and our spatial audio feature f^A , such that $f^{AV} = [f^A || f^V]$. Doing this late fusion of the visual and spatial audio features allows our pose predictor to learn important spatial correlations between the visual and audio modalities.

²Here, “viewpoint” refers to a microphone pose.

4.3. Model training

Binaural audio feature extractor training. Following [9, 16], given a target viewpoint \mathcal{T} and its ground-truth binaural audio segment $A_{\mathcal{T}}^B$, our NVAS model, whose encoder we use for our binaural feature extractor \mathcal{F}^B , predicts an estimate $\tilde{S}_{\mathcal{T}}^{\Delta}$ of the spectrogram of the ground-truth difference between the left and right channels of the target audio, $S_{\mathcal{T}}^{\Delta}$, such that $S_{\mathcal{T}}^{\Delta}$ is computed by performing STFT on $A_{\mathcal{T}}^l - A_{\mathcal{T}}^r$. With this formulation, the model is not required to predict the exact value of each entry in spectrogram, which greatly speeds up training while still enabling the model to learn strong binaural features due to its requirement of accurately predicting any inter-channel differences. We train the NVAS model and consequently, our binaural feature extractor \mathcal{F}^B , by computing \mathcal{L}^B , where \mathcal{L}^B is the L_1 loss between $S_{\mathcal{T}}^{\Delta}$ and $\tilde{S}_{\mathcal{T}}^{\Delta}$, such that

$$\mathcal{L}^B = \|\tilde{S}_{\mathcal{T}}^{\Delta} - S_{\mathcal{T}}^{\Delta}\|_1. \quad (1)$$

Camera pose estimator training. Given an RGB image pair (I_s, I_t) and the corresponding relative camera pose ground-truths $(P_{s \rightarrow t}, P_{t \rightarrow s})$, we train our audio-visual camera pose predictor \mathcal{F}^P using \mathcal{L}^P , where \mathcal{L}^P is the mean of the pose prediction loss $L_{s \rightarrow t}^P$ for $P_{t \rightarrow s}$ and its converse $L_{t \rightarrow s}^P$, corresponding to the prediction loss for $P_{t \rightarrow s}$, such that

$$\mathcal{L}^P = L_{s \rightarrow t}^P + L_{t \rightarrow s}^P \quad (2)$$

Following [14], our pose prediction loss L^P has two components, measuring the error in the rotation and translation predictions, respectively.

5. Experiments

We present experiments validating our model on two datasets, Ego-Exo4D [20] and HM3D-SoundSpaces [7, 46].

5.1. Experimental Setup

Datasets. To assess our method’s performance on real-world data, we first train and evaluate our models on the **Ego-Exo4D dataset** [20], using all 132 hours of egocentric sequences for which there are audio recordings (Ego-Exo4D’s exo cameras are static and hence not relevant for pose estimation). Audio in Ego-Exo4D is captured with 7 microphones on the Aria glasses, which provide synchronized multichannel audio and precise camera pose annotations. The data spans a diverse range of scenarios, motions, and activities, including indoor navigation, social interactions, and object manipulation, enabling evaluation across varied acoustic conditions like speech vs. object sounds, and foreground sounds vs. ambient noise, and visual conditions such as occlusion and lighting changes.

To generate our dataset, we uniformly sample frame pairs that are one second apart, ensuring sufficient motion while

maintaining temporal continuity. We follow the official Ego-Exo4D data splits, ensuring that frame pairs used for training and testing are sampled from entirely disjoint video subsets, fully preventing cross-split overlap during evaluation.

Secondly, to enable direct comparison with SLfM [9], which generates camera orientation and sound source locations, we additionally train and evaluate our approach on the Habitat-Matterport3D SoundSpaces (**HM3D-SS** **dataset**) [9, 46], which combines Habitat-Matterport3D’s photorealistic indoor scenes with the SoundSpaces [7] framework in order to produce realistic spatial audio in simulation. We follow the same data splits and scene configurations used in the SLfM work.

Finally, to assess robustness to corrupted visual inputs, we also generate a **corrupted test set** for each of the above datasets by applying a random combination of photometric and geometric transformations to each frame, where both the chosen transformations and their strengths are randomly decided. The set of possible perturbations includes Gaussian blur, Gaussian noise, and color jitter (brightness, contrast, saturation, and hue adjustments). See Table 3 for examples. These degradations include both standard corruption types used in prior robustness work [21, 28, 31, 34] as well as more extreme perturbations that occur when the transformations are applied with full strength, and simulate unexpected visual failures, enabling evaluation under both typical and worst-case visual conditions.

Baselines. We compare against the following baselines and state-of-the-art methods:

- **Chance:** this is a heuristic that outputs the mean of the ground-truth relative camera poses from the validation set, as its prediction
- **Naive Audio Camera Pose (NA-CP):** this baseline predicts the relative camera pose by replacing the RGB inputs to a Reloc3r [14] model, with corresponding multi-channel audio spectrograms, and finetuning it to predict estimates of the corresponding ground-truth camera poses
- **Direction-of-arrival Camera Pose (DOA-CP):** this baseline first computes the direction the direction-of-arrival (DoA) spectrum, and then predicts the relative camera pose by processing the DoA spectrum using a stack of linear layers
- **Reloc3r [14]:** a state-of-the-art vision-only relative camera pose predictor that takes pairs of RGB images as inputs and uses a transformer encoder-decoder model to predict the camera pose for the image pair, in both directions
- **Reloc3r [14]-AV:** an audio-visual version of Reloc3r that performs late fusion (cf. Sec. 4.2) of Reloc3r’s visual features and the audio features from the corresponding layer of our NA-CP baseline, and feeds the fused features to Reloc3r’s pose prediction head to estimate the relative camera

Table 1. Comparison of relative camera pose estimation performance on Ego-Exo4D dataset validation split. We report AUC@5, AUC@10, and AUC@20 metrics for rotation only, translation only, and total based on the maximum of the rotation and translation error. Best performing results are in bold, and second best results are underlined. All gains over baselines and ablations are statistically significant ($p \leq 0.05$).

Methods	Rotation Only			Translation Only			Total		
	AUC@5	AUC@10	AUC@20	AUC@5	AUC@10	AUC@20	AUC@5	AUC@10	AUC@20
<i>Audio Only</i>									
Chance	<u>19.02</u>	<u>33.33</u>	50.03	0.06	0.26	1.11	0.02	0.12	0.76
NA-CP Model	18.83	33.27	<u>50.05</u>	<u>0.07</u>	<u>0.29</u>	<u>1.16</u>	<u>0.02</u>	<u>0.12</u>	0.72
DOA CP Model	19.07	33.37	50.07	0.09	0.37	1.38	0.03	0.14	0.78
<i>Audio + Vision</i>									
Reloc3r [14]	37.35	53.62	68.98	0.73	2.63	7.77	0.57	2.33	7.33
Reloc3r [14]-AV	37.10	53.30	68.72	0.88	2.97	8.53	0.69	2.65	8.07
Ours w/o DOA	37.48	53.45	68.88	<u>0.96</u>	<u>3.21</u>	<u>8.92</u>	<u>0.75</u>	<u>2.86</u>	<u>8.41</u>
Ours w/o Binaural	<u>37.99</u>	<u>53.87</u>	<u>69.04</u>	0.93	3.12	8.80	0.74	2.80	8.34
Ours	38.54	54.49	69.61	1.03	3.36	9.34	0.81	2.99	8.82
<i>Audio + Corrupted Vision</i>									
Reloc3r [14]	25.17	38.88	52.80	0.34	1.28	4.28	0.21	1.00	3.66
Reloc3r [14]-AV	26.17	39.76	53.59	0.43	1.57	4.96	0.29	1.27	4.36
Ours w/o DOA	26.14	39.76	53.71	<u>0.45</u>	1.61	5.06	<u>0.31</u>	1.29	4.42
Ours w/o Binaural	<u>26.56</u>	<u>40.06</u>	<u>53.81</u>	0.44	<u>1.62</u>	<u>5.10</u>	0.29	<u>1.30</u>	<u>4.48</u>
Ours	27.17	40.66	54.46	0.49	1.77	5.45	0.35	1.44	4.80

Table 2. Results on the HM3D-SS dataset test split. We report rotation accuracy using mean absolute error (MAE ($^{\circ}$)) for the original data (left) and corrupted visual signals (right), following the evaluation protocol of SLfM [9]. Lower values are better. All gains over baselines and ablations are statistically significant ($p \leq 0.05$).

Method	Original	Corrupted
Chance	29.41	—
SLfM [9]	0.77	—
NA-CP Model	2.56	—
DOA-CP Model	28.63	—
Reloc3r [14]	0.09	3.83
Reloc3r-AV [14]	0.09	3.28
Ours w/o DOA	0.08	2.78
Ours w/o Binaural	0.08	2.66
Ours	0.06	2.46

pose. We finetune this model using pairs of audio-visual inputs and relative camera pose ground-truths.

Evaluation metrics. Following previous research [14, 49, 54, 60], we evaluate our model on the Ego-Exo4D dataset using AUC@5/10/20. These metrics compute the area under the accuracy curve (AUC) for camera pose estimation, with thresholds of 5, 10 and 20 degrees on the maximum

angular error in the rotation and translation predictions. This provides a comprehensive measure of relative pose accuracy across varying error tolerance levels.

For experiments on the HM3D-SS dataset, we strictly follow the evaluation protocol used in prior work [9] and only report the mean absolute error (MAE) in predictions of the rotation azimuth. This ensures a fair and consistent comparison across methods.

5.2. Results

We present the results for both datasets, including their visually corrupted variants, and then provide analysis of what audio properties are most and least amenable to augmenting vision for camera pose estimation.

5.2.1. Audio-visual relative camera pose estimation

Table 1 reports relative camera pose estimation results on the Ego-Exo4D test split,³ and Figure 3 shows qualitative examples. Among audio-only models, the DOA-CP model achieves the strongest overall performance, with higher AUC scores across most thresholds compared to both the mean baseline and the naive audio model. This demonstrates that

³Note that the SLfM [9] method is not applicable to Ego-Exo4D because when it jointly trains for sound source localization and camera motion, it requires ground truth direction-of-arrival values, which Ego-Exo4D does not provide.

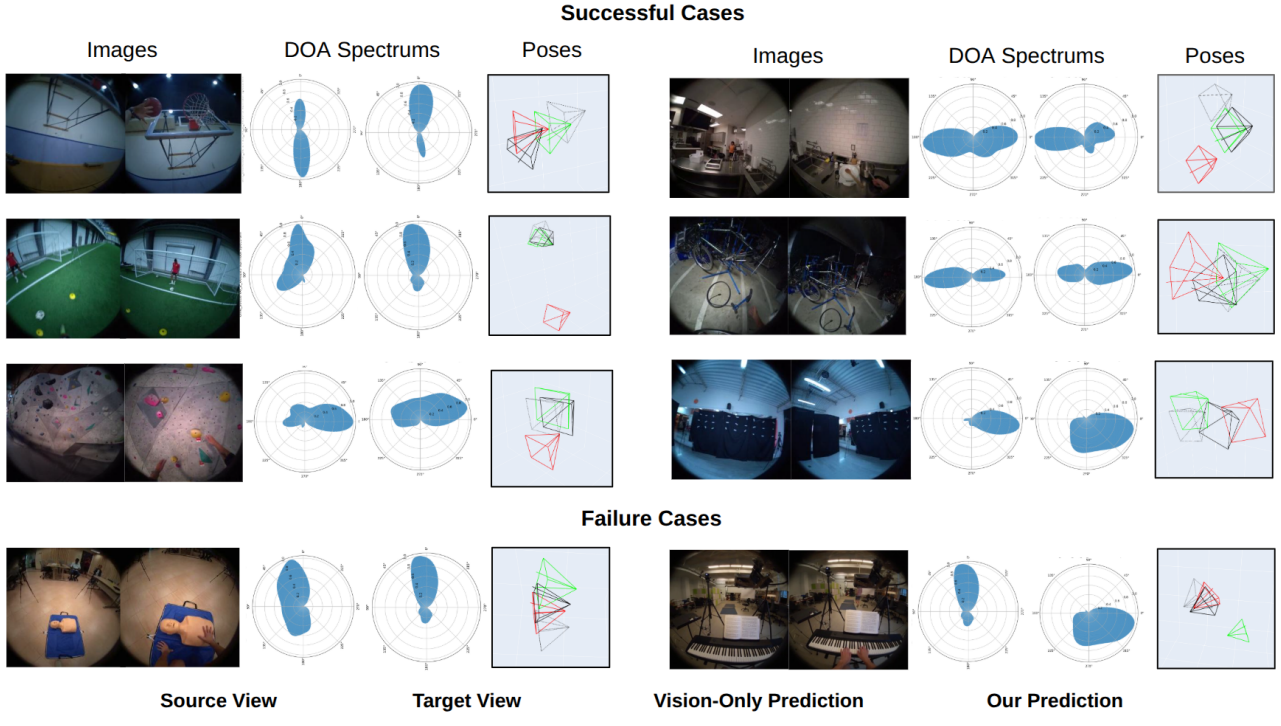


Figure 3. Qualitative examples of our audio-visual method outperforming a vision-only state-of-the-art relative camera pose estimation model. Our model performs well when there are consistent audio signals in the scene that aid in localization such as in the dancing example in the third row, where the sound of music is consistent throughout the entire video. Some failure cases of our model include when audio signals change between frames, but the camera does not move, like in the example on the bottom right, where the musician doesn't start playing music til the second frame.

direction-of-arrival (DOA) features extracted from multi-channel raw audio provide meaningful geometric cues for estimating relative pose, even without visual supervision.

When combining audio information with visual inputs, our approach outperforms all of our baselines and ablations with statistical significance ($p \leq 0.05$). Using only naive audio embeddings yields only minor gains in overall AUC, while performing worse than the baseline when focusing on rotation only. We can see that incorporating structured audio representations leads to consistent improvements across both rotation and translation metrics. Specifically, the addition of DOA features substantially enhances rotation accuracy, reflecting their ability to encode spatial geometry complementary to vision, while the binaural embeddings provide cues that improve translation estimation. Our full model achieves the highest total AUC across all thresholds, demonstrating the benefits of jointly leveraging both embeddings.

Furthermore, Table 1 shows that under corrupted vision conditions (bottom third of the table), our model maintains significantly higher performance than all baselines, highlighting its robustness when visual cues are degraded. These results collectively confirm that our multi-embedding fusion not only improves overall accuracy but also enhances cross-

modal reliability in challenging visual environments. Table 3 breaks down the relative accuracy for our method and its vision-only counterpart for each type of image corruption.

From Figure 3, we can see the impact that ambient audio has across many scenarios. Our method can adapt to sudden changes in pose that seem to throw off our vision-only model. There are a few cases where our method struggles, though, specifically when sudden changes in audio occur when the camera is not moving, or if there is minimal change in rotation or translation.

Table 2 shows the results on the HM3D-SS dataset, for both the original data (left) and the visually corrupted (right). We can see our model achieves the lowest mean absolute rotation error, outperforming both the state-of-the-art SLfM [9] and the Reloc3r [14] baseline in both normal and corrupted visual settings. While the improvement over the visual-only baseline on the original image data is minimal, this is largely due to the controlled nature of HM3D-SS scenes, where the visual signal alone is highly informative. This reinforces our emphasis on real-world video as a more challenging and essential testbed.

We also observe that the DOA Camera Pose model performs poorly in this setting, which may stem from inaccu-

Table 3. AUC@20 scores demonstrating robustness under different visual corruption scenarios, with corresponding visualizations below the table specifying the parameters used to evaluate performance. Our method consistently outperforms the baseline.

Corruption Method	Vision Only	Ours
Gaussian Blur	4.08	5.52
Gaussian Noise	2.63	3.47
Color Jitter	6.20	7.64

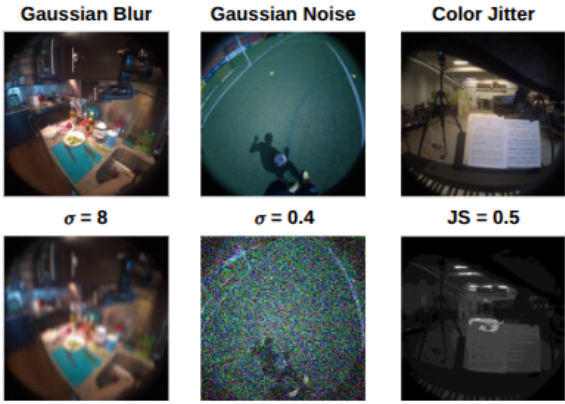


Table 4. Impact of scene audio characteristics on multimodal camera pose estimation performance. We evaluate camera pose estimation across eight Ego-Exo4D scenarios with varying audio characteristics. The second column indicates the most dominant audio types present in each scenario. The rightmost columns reports the percentage of frames where our method outperforms the vision-only (Reloc3r) baseline.

Scenario	Audio type(s)	Audio helps? (%)
Soccer	★ ■ ▲	84.63
Music	●	81.40
Bike Repair	◆ ■ ▲	79.55
Rock Climbing	★ ●	79.41
Basketball	★ ◆ ▲	72.15
Health	◆ ■	67.16
Dance	● ▲	66.14
Cooking	◆ ■	64.13

Audio Types: ★ Far-field ◆ Near-field / Egocentric ● Dominant Single Sound ■ Low Audio Signal ▲ Frequent Sound Changes

racies in how direction-of-arrival features are computed in simulation and the absence of precise microphone position parameters in the SoundSpaces [7] configuration. Nonetheless, our DOA-enhanced fusion model consistently surpasses the naive audio variant and vision-only baseline, suggesting that DOA cues remain beneficial even under imperfect calibration and strong visual dominance.

5.2.2. Analysis of passive scene audio characteristics

Table 4 demonstrates the robustness of our method across diverse acoustic conditions in the Ego-Exo4D dataset. We annotate each scenario with its predominant audio characteristics observed in the data, which includes far-field source audio (distant sound sources), near-field or egocentric audio (sounds proximate to the camera), dominant single sound source, low/minimal audio signal, and frequent sound changes between consecutive frames.

Our method most frequently outperforms its vision-only counterpart when sound sources are spatially distributed across the scene. In Soccer, our method achieves better results in 84.63% of frame pairs. Despite challenging conditions with far-field audio, low signal, and frequent changes, the spatially diverse sounds (ball impacts, player movements, background conversations) provide robust directional cues for pose estimation. Similarly, Music (81.40%) and Bike Repair (79.55%) benefit from spatially localized sound sources that remain consistent as the camera moves. In contrast, Cooking (64.13%) and Dance (66.14%) show healthy but more moderate gains due to limited spatial variation from repetitive localized sounds or stationary sound sources.

Overall, our approach provides the most reliable improvements over our vision-only baseline when sound sources exhibit spatial diversity or consistent localization. Our approach achieves consistent performance gains across diverse acoustic conditions.

6. Conclusion

We present a multimodal approach for relative camera pose estimation in video that exploits spatial cues from multichannel audio. Our method achieves state-of-the-art performance among audio-visual baselines on both real-world and simulated settings, demonstrating that ambient audio contains rich spatial structure to complement visual signals for a classic spatial vision tasks.

While our approach is effective, it has some limitations that present opportunities for future work. Translation estimation remains challenging in visually degraded or acoustically complex scenarios. In addition, it would be interesting to extend the model to explicitly gate the audio’s influence depending on its properties (e.g., stationarity). Despite these challenges, our work establishes that audio-visual fusion substantially improves pose estimation across diverse acoustic conditions. We hope this work motivates further research in leveraging sound for geometric reasoning and robust scene understanding.

References

[1] Triantafyllos Afouras, Andrew Owens, Joon Son Chung, and Andrew Zisserman. Self-supervised learning of audio-visual objects from video. In *Computer Vision–ECCV 2020: 16th European Conference, Glasgow, UK, August 23–28, 2020, Proceedings, Part XVIII 16*, pages 208–224. Springer, 2020. [2](#)

[2] Relja Arandjelovic and Andrew Zisserman. Look, listen and learn. *2017 IEEE International Conference on Computer Vision (ICCV)*, pages 609–617, 2017. [2](#)

[3] Eduardo Arnold, Jamie Wynn, Sara Vicente, Guillermo Garcia-Hernando, Aron Monszpart, Victor Adrian Prisacariu, Daniyar Turmukhambetov, and Eric Brachmann. Map-free visual relocalization: Metric pose relative to a single image. In *ECCV*, 2022. [2](#)

[4] Gilad Baruch, Zhiyuan Chen, Afshin Dehghan, Tal Dimry, Yuri Feigin, Peter Fu, Thomas Gebauer, Brandon Joffe, Daniel Kurz, Arik Schwartz, and Elad Shulman. Arkitscenes - a diverse real-world dataset for 3d indoor scene understanding using mobile rgb-d data. In *NeurIPS*, 2021. [2](#)

[5] Ruojin Cai, Jason Y Zhang, Philipp Henzler, Zhengqi Li, Noah Snavely, and Ricardo Martin-Brualla. Can generative video models help pose estimation? In *CVPR*, 2025. [2](#)

[6] Angel Chang, Angela Dai, Thomas Funkhouser, Maciej Halber, Matthias Niessner, Manolis Savva, Shuran Song, Andy Zeng, and Yinda Zhang. Matterport3d: Learning from rgb-d data in indoor environments. *International Conference on 3D Vision (3DV)*, 2017. [2](#)

[7] Changan Chen, Carl Schissler, Sanchit Garg, Philip Kobernik, Alexander Clegg, Paul Calamia, Dhruv Batra, Philip W Robinson, and Kristen Grauman. Soundspace 2.0: A simulation platform for visual-acoustic learning. In *NeurIPS 2022 Datasets and Benchmarks Track*, 2022. [1, 2, 5, 8](#)

[8] Changan Chen, Alexander Richard, Roman Shapovalov, Vamsi Krishna Ithapu, Natalia Neverova, Kristen Grauman, and Andrea Vedaldi. Novel-view acoustic synthesis. In *Proceedings of the IEEE/CVF Conference on Computer Vision and Pattern Recognition*, pages 6409–6419, 2023. [4](#)

[9] Ziyang Chen, Shengyi Qian, and Andrew Owens. Sound localization from motion: Jointly learning sound direction and camera rotation. In *International Conference on Computer Vision (ICCV)*, 2023. [1, 2, 4, 5, 6, 7, 12](#)

[10] Jesper Haahr Christensen, Sascha Hornauer, and Stella X. Yu. Batvision: Learning to see 3d spatial layout with two ears. *2020 IEEE International Conference on Robotics and Automation (ICRA)*, pages 1581–1587, 2019. [1, 2](#)

[11] Angela Dai, Angel X. Chang, Manolis Savva, Maciej Halber, Thomas Funkhouser, and Matthias Niessner. Scannet: Richly-annotated 3d reconstructions of indoor scenes. In *Proc. Computer Vision and Pattern Recognition (CVPR), IEEE*, 2017. [2](#)

[12] Dima Damen, Hazel Doughty, Giovanni Maria Farinella, Sanja Fidler, Antonino Furnari, Evangelos Kazakos, Davide Moltisanti, Jonathan Munro, Toby Perrett, Will Price, et al. The epic-kitchens dataset: Collection, challenges and baselines. *IEEE Transactions on Pattern Analysis and Machine Intelligence*, 43(11):4125–4141, 2020. [2](#)

[13] Yaqing Ding, Viktor Kocur, Vaclav Vavra, Zuzana Berger Haladova, Jian Yang, Torsten Sattler, and Zuzana Kukelova. Reposed: Efficient relative pose estimation with known depth information. *arXiv preprint arXiv:2501.07742*, 2025. [2](#)

[14] Siyan Dong, Shuzhe Wang, Shaohui Liu, Lulu Cai, Qingnan Fan, Juho Kannala, and Yanchao Yang. Reloc3r: Large-scale training of relative camera pose regression for generalizable, fast, and accurate visual localization. In *Proceedings of the IEEE/CVF Conference on Computer Vision and Pattern Recognition (CVPR)*, pages 16739–16752, 2025. [1, 2, 3, 4, 5, 6, 7, 12, 13](#)

[15] Chuang Gan, Yiwei Zhang, Jiajun Wu, Boqing Gong, and Joshua B. Tenenbaum. Look, listen, and act: Towards audio-visual embodied navigation. In *ICRA*, 2020. [1, 2](#)

[16] Ruohan Gao and Kristen Grauman. 2.5d visual sound. In *2019 IEEE/CVF Conference on Computer Vision and Pattern Recognition (CVPR)*, pages 324–333, 2019. [4, 5, 12](#)

[17] Ruohan Gao, Changan Chen, Ziad Al-Halah, Carl Schissler, and Kristen Grauman. Visualechoes: Spatial image representation learning through echolocation. In *ECCV*, 2020. [1, 2, 4](#)

[18] Mariana-Iuliana Georgescu, Eduardo Fonseca, Radu Tudor Ionescu, Mario Lucic, Cordelia Schmid, and Anurag Arnab. Audiovisual masked autoencoders. *arXiv preprint arXiv:2212.05922*, 2022. [2](#)

[19] Yuan Gong, Andrew Rouditchenko, Alexander H. Liu, David Harwath, Leonid Karlinsky, Hilde Kuehne, and James R. Glass. Contrastive audio-visual masked autoencoder. In *The Eleventh International Conference on Learning Representations*, 2023. [2](#)

[20] Kristen Grauman, Andrew Westbury, Lorenzo Torresani, Kris Kitani, Jitendra Malik, Triantafyllos Afouras, Kumar Ashutosh, Vijay Baiyya, Siddhant Bansal, Bikram Boote, et al. Ego-exo4d: Understanding skilled human activity from first-and third-person perspectives. In *Proceedings of the IEEE/CVF Conference on Computer Vision and Pattern Recognition*, pages 19383–19400, 2024. [2, 4, 5](#)

[21] Dan Hendrycks and Thomas Dietterich. Benchmarking neural network robustness to common corruptions and perturbations. *arXiv preprint arXiv:1903.12261*, 2019. [5](#)

[22] Po-Yao Huang, Vasu Sharma, Hu Xu, Chaitanya Ryali, Haoqi Fan, Yanghao Li, Shang-Wen Li, Gargi Ghosh, Jitendra Malik, and Christoph Feichtenhofer. Mavil: Masked audio-video learners. *arXiv preprint arXiv:2212.08071*, 2022. [2](#)

[23] Bruno Korbar, Du Tran, and Lorenzo Torresani. Cooperative learning of audio and video models from self-supervised synchronization. *Advances in Neural Information Processing Systems*, 31, 2018. [2](#)

[24] Wenbin Li, Sajad Saeedi, John McCormac, Ronald Clark, Dimos Tzoumanikas, Qing Ye, Yuzhong Huang, Rui Tang, and Stefan Leutenegger. Interiornet: Mega-scale multi-sensor photo-realistic indoor scenes dataset. In *British Machine Vision Conference (BMVC)*, 2018. [2](#)

[25] Zhengqi Li and Noah Snavely. Megadepth: Learning single-view depth prediction from internet photos. In *Proceedings of the IEEE conference on computer vision and pattern recognition*, pages 2041–2050, 2018. [2](#)

[26] Zhaojian Li, Bin Zhao, and Yuan Yuan. Cyclic learning for binaural audio generation and localization. In *Proceedings of the IEEE/CVF Conference on Computer Vision and Pattern Recognition (CVPR)*, pages 26669–26678, 2024. 2

[27] Lu Ling, Yichen Sheng, Zhi Tu, Wentian Zhao, Cheng Xin, Kun Wan, Lantao Yu, Qianyu Guo, Zixun Yu, Yawen Lu, et al. DL3dv-10k: A large-scale scene dataset for deep learning-based 3d vision. In *Proceedings of the IEEE/CVF Conference on Computer Vision and Pattern Recognition*, pages 22160–22169, 2024. 2

[28] Jiawei Liu, Zhijie Wang, Lei Ma, Chunrong Fang, Tongtong Bai, Xufan Zhang, Jia Liu, and Zhenyu Chen. Benchmarking object detection robustness against real-world corruptions. *International Journal of Computer Vision*, 132(10):4398–4416, 2024. 5

[29] Xingchen Liu, Piyush Tayal, Jianyuan Wang, Jesus Zarzar, Tom Monnier, Konstantinos Tertikas, Jiali Duan, Antoine Toisoul, Jason Y. Zhang, Natalia Neverova, Andrea Vedaldi, Roman Shapovalov, and David Novotny. Uncommon objects in 3d. In *arXiv*, 2024. 2

[30] Thibaut Loiseau, Guillaume Bourmaud, and Vincent Lepetit. AlligatOr: Pre-training through co-visibility segmentation for relative camera pose regression. *CoRR*, abs/2503.07561, 2025. 2

[31] Sihan Ma, Jing Zhang, Qiong Cao, and Dacheng Tao. Posebench: Benchmarking the robustness of pose estimation models under corruptions. *ArXiv*, abs/2406.14367, 2024. 5

[32] Sagnik Majumder, Ziad Al-Halah, and Kristen Grauman. Learning spatial features from audio-visual correspondence in egocentric videos. In *Proceedings of the IEEE/CVF Conference on Computer Vision and Pattern Recognition (CVPR)*, pages 27058–27068, 2024. 4

[33] Anna Min, Ziyang Chen, Hang Zhao, and Andrew Owens. Supervising sound localization by in-the-wild egomotion. In *Proceedings of the Computer Vision and Pattern Recognition Conference*, pages 23936–23946, 2025. 2

[34] Eric Mintun, Alexander Kirillov, and Saining Xie. On interaction between augmentations and corruptions in natural corruption robustness. In *Advances in Neural Information Processing Systems*, 2021. 5

[35] Piotr Mirowski, Andras Banki-Horvath, Keith Anderson, Denis Teplyashin, Karl Moritz Hermann, Mateusz Malinowski, Matthew Koichi Grimes, Karen Simonyan, Koray Kavukcuoglu, Andrew Zisserman, and Raia Hadsell. The streetlearn environment and dataset. *CoRR*, abs/1903.01292, 2019. 2

[36] Pedro Morgado, Yi Li, and Nuno Vasconcelos. Self-supervised generation of spatial audio for 360° video. *Advances in Neural Information Processing Systems*, 33:4733–4744, 2020. 2

[37] P. Morgado, Y. Li, and N. Vasconcelos. Learning representations from audio-visual spatial alignment. In *NeurIPS*, 2020. 4

[38] Jiquan Ngiam, Aditya Khosla, Mingyu Kim, Juhan Nam, Honglak Lee, and A. Ng. Multimodal deep learning. In *International Conference on Machine Learning*, 2011. 2

[39] Andrew Owens and Alexei A Efros. Audio-visual scene analysis with self-supervised multisensory features. In *Proceedings of the European Conference on Computer Vision (ECCV)*, pages 631–648, 2018. 2

[40] Andrew Owens, Phillip Isola, Josh McDermott, Antonio Torralba, Edward H Adelson, and William T Freeman. Visually indicated sounds. In *Proceedings of the IEEE conference on computer vision and pattern recognition*, pages 2405–2413, 2016. 2

[41] Andrew Owens, Jiajun Wu, Josh H. McDermott, William T. Freeman, and Antonio Torralba. Ambient sound provides supervision for visual learning. In *European Conference on Computer Vision*, 2016. 2

[42] Kranti Kumar Parida, Siddharth Srivastava, and Gaurav Sharma. Beyond mono to binaural: Generating binaural audio from mono audio with depth and cross modal attention. In *2022 IEEE/CVF Winter Conference on Applications of Computer Vision (WACV)*, pages 2151–2160, 2022. 4

[43] Andres Perez-Lopez. pysofaconventions: Python implementation of the SOFA specification, 2019. 4

[44] Xavi Puig, Eric Undersander, Andrew Szot, Mikael Dallaire Cote, Ruslan Partsey, Jimmy Yang, Ruta Desai, Alexander William Clegg, Michal Hlavac, Tiffany Min, Theo Gervet, Vladimir Vondrus, Vincent-Pierre Berges, John Turner, Oleksandr Maksymets, Zsolt Kira, Mrinal Kalakrishnan, Jitendra Malik, Devendra Singh Chaplot, Unnat Jain, Dhruv Batra, Akshara Rai, and Roozbeh Mottaghi. Habitat 3.0: A co-habitat for humans, avatars and robots, 2023. 2

[45] Senthil Purushwalkam, S. V. A. Gari, Vamsi Krishna Ithapu, Carl Schissler, Philip Robinson, Abhinav Kumar Gupta, and Kristen Grauman. Audio-visual floorplan reconstruction. *2021 IEEE/CVF International Conference on Computer Vision (ICCV)*, pages 1163–1172, 2020. 1, 2

[46] Santhosh Kumar Ramakrishnan, Aaron Gokaslan, Erik Wijmans, Oleksandr Maksymets, Alexander Clegg, John M Turner, Eric Undersander, Wojciech Galuba, Andrew Westbury, Angel X Chang, Manolis Savva, Yili Zhao, and Dhruv Batra. Habitat-matterport 3d dataset (HM3d): 1000 large-scale 3d environments for embodied AI. In *Thirty-fifth Conference on Neural Information Processing Systems Datasets and Benchmarks Track*, 2021. 1, 2, 5

[47] Chris Rockwell, Nilesh Kulkarni, Linyi Jin, Jeong Joon Park, Justin Johnson, and David F. Fouhey. Far: Flexible, accurate and robust 6dof relative camera pose estimation. In *CVPR*, 2024. 2

[48] Daniele Salvati, Carlo Drioli, and Gian Luca Foresti. Incoherent frequency fusion for broadband steered response power algorithms in noisy environments. *IEEE Signal Processing Letters*, 21(5):581–585, 2014. 4

[49] Paul-Edouard Sarlin, Daniel DeTone, Tomasz Malisiewicz, and Andrew Rabinovich. SuperGlue: Learning feature matching with graph neural networks. In *CVPR*, 2020. 2, 6

[50] Manolis Savva, Abhishek Kadian, Oleksandr Maksymets, Yili Zhao, Erik Wijmans, Bhavana Jain, Julian Straub, Jia Liu, Vladlen Koltun, Jitendra Malik, Devi Parikh, and Dhruv Batra. Habitat: A Platform for Embodied AI Research. In *Proceedings of the IEEE/CVF International Conference on Computer Vision (ICCV)*, 2019. 2

[51] R. Schmidt. Multiple emitter location and signal parameter estimation. *IEEE Transactions on Antennas and Propagation*, 34(3):276–280, 1986. 4

[52] Noah Snavely, Steven M. Seitz, and Richard Szeliski. Photo tourism: Exploring photo collections in 3d. In *SIGGRAPH Conference Proceedings*, pages 835–846, New York, NY, USA, 2006. ACM Press. 2

[53] Julian Straub, Thomas Whelan, Lingni Ma, Yufan Chen, Erik Wijmans, Simon Green, Jakob J. Engel, Raul Mur-Artal, Carl Ren, Shobhit Verma, Anton Clarkson, Mingfei Yan, Brian Budge, Yajie Yan, Xiaqing Pan, June Yon, Yuyang Zou, Kimberly Leon, Nigel Carter, Jesus Briales, Tyler Gillingham, Elias Mueggler, Luis Pesqueira, Manolis Savva, Dhruv Batra, Hauke M. Strasdat, Renzo De Nardi, Michael Goesele, Steven Lovegrove, and Richard Newcombe. The Replica dataset: A digital replica of indoor spaces. *arXiv preprint arXiv:1906.05797*, 2019. 1, 2

[54] Jiaming Sun, Zehong Shen, Yuang Wang, Hujun Bao, and Xiaowei Zhou. LoFTR: Detector-free local feature matching with transformers. *CVPR*, 2021. 2, 6

[55] Pei Sun, Henrik Kretzschmar, Xerxes Dotiwalla, Aurelien Chouard, Vijaysai Patnaik, Paul Tsui, James Guo, Yin Zhou, Yuning Chai, Benjamin Caine, Vijay Vasudevan, Wei Han, Jiquan Ngiam, Hang Zhao, Aleksei Timofeev, Scott Ettinger, Maxim Krivokon, Amy Gao, Aditya Joshi, Yu Zhang, Jonathon Shlens, Zhifeng Chen, and Dragomir Anguelov. Scalability in perception for autonomous driving: Waymo open dataset. In *Proceedings of the IEEE/CVF Conference on Computer Vision and Pattern Recognition (CVPR)*, 2020. 2

[56] Andrew Szot, Alex Clegg, Eric Undersander, Erik Wijmans, Yili Zhao, John Turner, Noah Maestre, Mustafa Mukadam, Devendra Chaplot, Oleksandr Maksymets, Aaron Gokaslan, Vladimir Vondrus, Sameer Dharur, Franziska Meier, Wojciech Galuba, Angel Chang, Zsolt Kira, Vladlen Koltun, Jitendra Malik, Manolis Savva, and Dhruv Batra. Habitat 2.0: Training home assistants to rearrange their habitat. In *Advances in Neural Information Processing Systems (NeurIPS)*, 2021. 2

[57] Bart Thomee, David A Shamma, Gerald Friedland, Benjamin Elizalde, Karl Ni, Douglas Poland, Damian Borth, and Li-Jia Li. Yfcc100m: The new data in multimedia research. *Communications of the ACM*, 59(2):64–73, 2016. 2

[58] Jianyuan Wang, Minghao Chen, Nikita Karaev, Andrea Vedaldi, Christian Rupprecht, and David Novotny. Vggt: Visual geometry grounded transformer. In *Proceedings of the IEEE/CVF Conference on Computer Vision and Pattern Recognition*, 2025. 2

[59] Shuzhe Wang, Vincent Leroy, Yohann Cabon, Boris Chidlovskii, and Jerome Revaud. Dust3r: Geometric 3d vision made easy. In *CVPR*, 2024. 2

[60] Yifan Wang, Xingyi He, Sida Peng, Dongli Tan, and Xiaowei Zhou. Efficient LoFTR: Semi-dense local feature matching with sparse-like speed. In *CVPR*, 2024. 6

[61] Felix Wimbauer, Weirong Chen, Dominik Muhle, Christian Rupprecht, and Daniel Cremers. Anycam: Learning to recover camera poses and intrinsics from casual videos. In *Proceedings of the Computer Vision and Pattern Recognition Conference*, pages 16717–16727, 2025. 2

[62] Xinyi Wu, Zhenyao Wu, Lili Ju, and Song Wang. Binaural audio-visual localization. In *AAAI*, pages 2961–2968, 2021. 2

[63] Ning Xu, Linjie Yang, Yuchen Fan, Jianchao Yang, Dingcheng Yue, Yuchen Liang, Brian Price, Scott Cohen, and Thomas Huang. Youtube-vos: Sequence-to-sequence video object segmentation. In *Proceedings of the European conference on computer vision (ECCV)*, pages 585–601, 2018. 2

[64] Karren Yang, Bryan Russell, and Justin Salamon. Telling left from right: Learning spatial correspondence of sight and sound. In *CVPR*, 2020. 4

[65] Karren Yang, Michael Firman, Eric Brachmann, and Clement Godard. Camera pose estimation and localization with active audio sensing. In *European Conference on Computer Vision*, pages 271–291. Springer, 2022. 1, 2

[66] Yao Yao, Zixin Luo, Shiwei Li, Jingyang Zhang, Yufan Ren, Lei Zhou, Tian Fang, and Long Quan. Blendedmvs: A large-scale dataset for generalized multi-view stereo networks. *Computer Vision and Pattern Recognition (CVPR)*, 2020. 2

[67] Chandan Yeshwanth, Yueh-Cheng Liu, Matthias Nießner, and Angela Dai. Scannet++: A high-fidelity dataset of 3d indoor scenes. In *Proceedings of the International Conference on Computer Vision (ICCV)*, 2023. 2

[68] Zhichao Yin and Jianping Shi. Geonet: Unsupervised learning of dense depth, optical flow and camera pose. In *Proceedings of the IEEE Conference on Computer Vision and Pattern Recognition (CVPR)*, 2018. 2

[69] Junyi Zhang, Charles Herrmann, Junhwa Hur, Varun Jampani, Trevor Darrell, Forrester Cole, Deqing Sun, and Ming-Hsuan Yang. MonST3r: A simple approach for estimating geometry in the presence of motion. In *The Thirteenth International Conference on Learning Representations*, 2025. 2

[70] Tinghui Zhou, Richard Tucker, John Flynn, Graham Fyffe, and Noah Snavely. Stereo magnification: Learning view synthesis using multiplane images. *arXiv preprint arXiv:1805.09817*, 2018. 2

Table 5. Mean of the ground-truth rotation and translation of the camera, expressed using angles, for different activity scenarios.

Scenario	Mean Rotation (°)	Mean Translation (°)
Basketball	43.29	40.07
Bike Repair	16.45	15.93
Cooking	14.76	14.07
Dance	40.98	40.38
Health	8.12	9.24
Music	7.29	8.09
Rock Climbing	39.41	32.39
Soccer	41.14	42.76
Total	18.35	17.94

7. Supplementary material

7.1. Implementation Details

Here, we provide our model’s training hyperparameters:

- Training epochs: 100
- Warmup epochs: 5
- Learning rate: 10^{-5}
- Minimum learning rate: 10^{-7}
- Batch size: 64
- Learning rate scheduler: Cosine annealing

Here, we provide the steps and parameters for processing the visual inputs for Reloc3r [14], specifically the Reloc3r-512 variant, which we use for all our experiments:

- Image size: 256×256
- Data augmentation methods: Random color jittering
- Number of encoder layers: 24
- Number of decoder layers: 12
- Number of layers in pose regression head: 4
- Embedding size: 1024

Here, we provide our audio processing parameters:

- Audio sample rate: 48 kHz
- Spectrogram size per channel: 512×96
- Sound clip length: 1000ms
- Number of FFT bins: 1024
- Number of sound sources we detect for DOA: 1

Here, we provide details of our binauralization model (Section 4.1 in main). We adopt the SLfM [9] architecture for the binauralizer, but modify it by removing the visual encoder and using a ResNet-18 audio encoder with an embedding size of 1024 for the binaural audio features. The model also incorporates an audio U-Net [16], following the design in SLfM [9].

To fuse our DOA spectrum and binaural embeddings, we first concatenate them into a single audio embedding of size $360 + 1024 = 1384$, where the feature size of the DoA and binaural embeddings are 360 and 1024, respectively. This joint audio embedding is then projected through a linear layer to produce a 768-dimensional audio representation. In parallel, the visual features extracted by the Reloc3r network

Table 6. Total AUC@20 for different audio clip durations. Using 1000ms audio leads to the best performance for our setup.

Sound Clip Size	60ms	500ms	1000ms
<i>Audio Only</i>			
NA-CP Model	0.68	0.69	0.72
DOA CP Model	0.68	0.72	0.78
<i>Audio + Vision</i>			
Reloc3r [14]-AV	7.83	7.38	8.07
Ours w/o DOA	7.63	7.84	8.41
Ours w/o Binaural	7.48	8.01	8.34
Ours	8.02	8.43	8.82

are passed through their own linear layer to produce a 768-dimensional visual embedding. The transformed visual and audio embeddings are then concatenated to form a joint multimodal representation, which is then fed into Reloc3r’s pose regression head. Finally, this fused embedding is used to predict the camera pose matrix.

7.2. More Analyses

7.2.1. Further Ego-Exo4D Dataset Analysis

As shown in Table 5, different scenarios exhibit widely varying amounts of camera motion. Activities like playing an instrument or performing COVID tests or CPR involve minimal movement, whereas sports and dynamic activities, such as basketball, soccer, rock climbing, and dancing, produce substantially higher motion. This highlights the broad diversity of scenarios captured in our dataset.

To annotate sound types for each scenario, we manually inspected subsets of videos within every scenario group and identified the dominant audio characteristics. Although the dataset is large, many videos were recorded in similar environments, and their audio profiles remained consistent. For example, in the Health scenario, most videos contained either minimal audio or egocentric narration, with other sound types appearing too infrequently to warrant inclusion in Table 4 in main. We applied this same process across all scenarios.

7.2.2. Additional Model Analyses

Impact of different audio clip lengths on model performance. We experimented with different sound clip lengths to determine which ones work best for our method. The potential advantage of using a very short time window (e.g., 60 ms) is that the audio is dominated by a single instantaneous acoustic event, which can help the model more easily isolate a single sound source and avoid the mixing that happens when multiple events overlap.

However, short clips are also limited, as they often contain too little acoustic variation to reveal meaningful spatial cues

Table 7. Total AUC scores across different temporal separations between frames in an input pair. Even though we perform our training uniformly using a 1 second difference between frames, our method generalizes across varying time differences.

Method	0.5s			1s			2s			4s		
	@5	@10	@20	@5	@10	@20	@5	@10	@20	@5	@10	@20
Reloc3r [14]	0.58	2.34	7.38	0.57	2.33	7.33	0.55	2.25	7.12	0.52	2.12	6.90
Ours	0.82	2.86	8.58	0.81	2.99	8.82	0.70	2.78	8.74	0.66	2.64	8.63

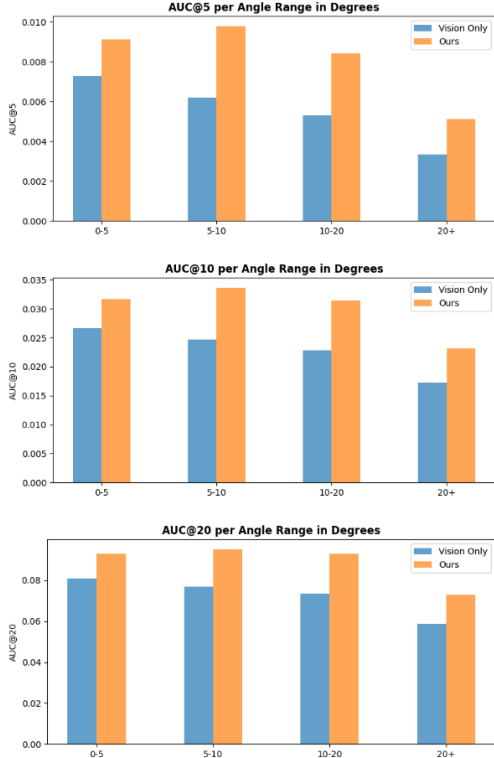


Figure 4. Our model performance compared against a SOTA vision-only baseline [14]. We evaluate our model’s performance across different ranges of the magnitude of the ground-truth relative camera pose, expressed in angles, where these ranges are $0\text{--}5^\circ$, $5\text{--}10^\circ$, $10\text{--}20^\circ$, and $20+^\circ$. We can clearly see that our model outperforms the baseline in all possible angle ranges.

about the environment, especially in scenes where sound sources are quiet, intermittent, or dominated by background noise. In contrast, longer sound clips can capture more acoustic structure (reverberation, reflections, changes in relative loudness, and continuous sound dynamics) that provide stronger indirect signals about camera motion. These longer windows can help the model form a more stable representation of how the camera is moving relative to the surrounding scene.

We did not extend our experiments beyond a 1 second window for a few reasons. First, as clip length increases, the correspondence between the audio window and the ground-truth relative pose becomes increasingly ambiguous: within

a long window, the camera may have moved significantly, making it unclear which portion of the audio should correspond to the target transformation. Second, longer windows increasingly entangle multiple independent sound events, which can blur the spatial cues that our model relies on.

From our results in Table 6, we can see that using 1000ms clips consistently worked the best for all of our methods.

Robustness to different magnitudes of target relative camera pose. Here, we evaluate our method against our vision-only model based on its ability to accurately predict estimates of target relative camera poses of different magnitudes. Figure 4 shows the results from this analysis. We note that across all AUC thresholds, our method outperforms our SOTA vision-only baseline [14] for different ranges of target camera pose magnitude, expressed using angles, including ranges with a mean greater than the overall mean magnitude of the ground-truth relative camera poses from our test set.

Robustness to different inter-frame temporal separations. In Table 7, we evaluate our model performance against Reloc3r for different sizes of the temporal separation between two frames in an input pair. Although our models are trained using frame pairs spaced one second apart, we find that this choice does not meaningfully limit generalization to larger temporal offsets. In evaluation, our audio-visual model not only outperforms the vision-only baseline across all AUC thresholds, but it also maintains stable performance as the frame gap increases, remaining consistent even at 4-second separations that were never seen during training. This indicates that our model can generalize to diverse frame rates in videos.

7.3. Ethical Considerations

Because our method relies on incidentally recorded ambient audio, it raises important privacy considerations. In particular, using audio for camera-pose estimation could enable unintended forms of environmental or bystander tracking. Any real-world deployment of systems built on this technology should require explicit user consent and should ensure that individuals understand that both the visual and acoustic environments they encounter may be processed. Future work should incorporate safeguards such as on-device processing, strict data-retention limits, and transparent opt-in mechanisms to prevent misuse in surveillance-adjacent settings.